DOI: https://doi.org/10.54966/g8sxvk67

Journal of Renewable Energies

Revue des Energies Renouvelables

Journal home page: https://revue.cder.dz/index.php/rer

Research paper

Three Hour Ahead PV Power Forecasting with Bidirectional Recurrent Networks: Insights into Monthly Variability

Ferial El Robrini [a,*], **Badia Amrouche** [a]

[a] *Laboratory of Electrical Systems and Remote Control (LabSET), Renewable Energies Department, Faculty of Technology, Blida 1 University, 09000, Algeria*

ARTICLE INFO

Article history:
Received October 3, 2024
Accepted January 29, 2025
Available online May 12, 2025
Published: June 26, 2025

Keywords:
Grid-connected photovoltaic power plant,
Long short-term memory,
Gated recurrent unit,
Bidirectional neural networks,
Forecasting,
Prediction.

ABSTRACT

Despite extensive research into PV power forecast models, their monthly performance is rarely thoroughly examined, creating gaps in our understanding of their accuracy and applicability across different times of the year. This paper focuses on evaluating the monthly performance of four predictive models designed for a three-hour forecast horizon. The studied models are based on distinct architectures of Recurrent Neural Networks (RNNs): Long Short-Term Memory (LSTM), Bidirectional LSTM (Bi-LSTM), Gated Recurrent Unit (GRU), and Bidirectional GRU (Bi-GRU). By analyzing statistical indicators across various months, we uncover seasonal fluctuations, with performance hitting its lowest points in winter (November and December) and peaking in summer (June to August). Notably, Bi-GRU consistently outperforms the other models, displaying lower error rates and higher accuracy across diverse months. As a result, it emerges as the preferred choice for forecasting due to its superior predictive capability. Additionally, we observe variations in daily performance across seasons, highlighting the complexities of data sequences and underscoring the importance of careful model selection. This research significantly contributes to the advancement of predictive modeling in time-series analysis, providing valuable insights into model performance and seasonal variations, and equipping practitioners and researchers with enhanced methodologies for improving forecast accuracy.

1. INTRODUCTION

Renewable energy sources are garnering significant attention, with solar photovoltaics (PV) emerging as a favored option due to its cleanliness, affordability, and widespread availability. As part of its energy transition program and exploration of solar energy potential, Algeria is actively shifting towards renewable energy sources. By the end of 2023, the country had reached a cumulative installed capacity

* *Corresponding author, E-mail address: elrobrini_ferial@univ-blida.dz / ferialelrobrini@gmail.com*

ISSN: 1112-2242 / EISSN: 2716-8247

of 436MW, including 24 grid-connected photovoltaic (PV) power plants generating 366.1 MW. Algeria has projected an additional 3200 MW of capacity in the coming years (Bilan des Capacités d'Energies Renouvelables Installées en Algérie à Fin 2023, 2024), as depicted in Fig.1, which shows the locations of operational and projected PV plants, highlighting Algeria's commitment to expanding its renewable energy infrastructure (Commissariat aux Energies Renouvelables et à l'Efficacité Energétique, 2020 ; Ministère de la Transition Energerique et des Energies Renouvelables, 2021 ; SONELGAZ-EnR, 2023).

This increasing prominence underscores the importance of efficiently predicting solar power plant output to mitigate the inherent stochasticity associated with these sources (Sampath Kumar, Gandhi, Rodríguez-Gallegos, & Srinivasan, 2020). Accurate prediction of PV power output and capacity value is paramount for effective energy management, decision-making processes, ensuring system security, meeting energy demands, and optimizing operational efficiency to ensure resource adequacy within the power system (Gandhi et al., 2020a ; Dolatabadi et al., 2024). Inadequate planning and allocation of resources may lead to insufficient reserve capacity to address unforeseen system contingencies, potentially compromising voltage stability, frequency, protection mechanisms, harmonics, rotor angle stability, and flexibility requirements. (Gandhi et al., 2020b)

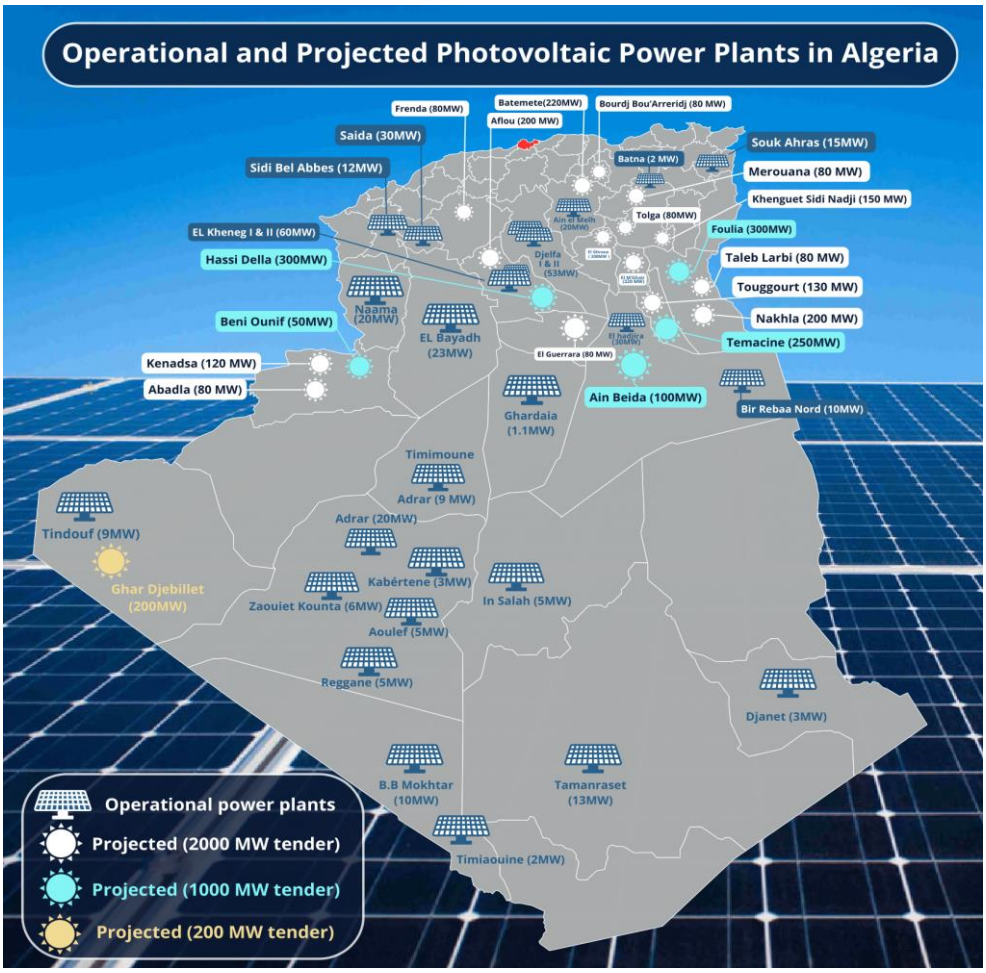

Fig 1. Operational and projected PV (Picture generated based on [7-9])

The availability of high-computational-capability processors coupled with access to baseline data confers a significant advantage to deep learning models for predicting solar power plant outputs. Predicting PV generation entails forecasting the future energy output of a specific PV station, a task influenced by various factors including spatial and temporal resolution (Raza, Nadarajah, & Ekanayake, 2016 ; Shab, 2022), geographical coordinates, meteorological conditions, seasonal fluctuations, solar

panel efficiency, power plant area, and employed solar energy conversion technologies. Predictive models leverage historical data analysis to discern trends, patterns, and correlations, thereby extrapolating this information to generate accurate projections or forecasts. The literature encompasses a plethora of photovoltaic power prediction models, each striving to enhance forecast accuracy while minimizing computational cost (Raza et al., 2016). These models are typically categorized into persistence methods (Ssekulima, Anwar, Al Hinai, & El Moursi, 2016 ; Yang, 2019), physical techniques (Raza et al., 2016), statistical approaches (empirical (Cryer & Chan, s.d. ; Huang, Korolkiewicz, Agrawal, & Boland, 2013), machine learning (Benmouiza & Cheknane, 2013, 2019 ; El Robrini & Amrouche, 2023 ; Khelifi, Guermoui, Rabehi, & Lalmi, 2020 ; Kuppusamy & Balaraman, 2024)), and hybrid methodologies models (Guermoui, Gairaa, Boland, & Arrif, 2021 ; Kushwaha & Pindoriya, 2019 ; Rabehi, Guermoui, & Lalmi, 2020).

2. LITERATURE REVIEW

During the last decades, numerous studies have been published on forecasting photovoltaic generation that exhibit significant differences, mainly due to the varied input datasets they utilize, including photovoltaic data, solar irradiation, temperature, air pressure, humidity, wind direction, and speed. Furthermore, these approaches vary in their forecasting horizons, techniques, and algorithms. In line with this, Table 1 provides a summary of relevant and recent approaches related to PV power forecasts, including their specifications and key contributions.

When examining the challenges of improving daily and intraday PV power forecasting models, we've identified several key research gaps. Firstly, current research tends to focus mainly on small-scale PV systems, overlooking the increasing significance of data from large-scale PV plants in the renewable energy sector. Secondly, most studies concentrate on very short-term (less than 1 hour) or medium-term (daily) forecasting, neglecting the crucial 2 to 4-hour timeframe necessary for conventional power plants to start up. This timeframe is essential for understanding effective photovoltaic energy compensation during peak hours. Additionally, only a few papers specifically address the performance of their predictive models across different months, failing to adequately assess the models' accuracy throughout the entire year. This work aims to explore the forecasting ability of deep learning techniques across different PV datasets. We utilized Long Short-Term Memory (LSTM), Bidirectional Long Short-Term Memory (Bi-LSTM), Gated Recurrent Unit (GRU), and Bidirectional GRU (Bi-GRU) to forecast intraday PV power. The distinctive contributions of this paper include:

- **Extended Forecasting horizon:** A forecasting horizon of three hours (3h) is used in this study. This extended timeframe offers valuable insights, especially in the context of energy compensation during peak hours, considering the startup durations of conventional power plants.
- **Seasonal Patterns Identification:** The predictive models may struggle to capture the underlying patterns in the data during certain times of the year, potentially due to factors such as increased volatility or changing dynamics. A detailed investigation of the model’s predictive behavior across the months is done.
- **Model Performance:** This paper compares the performance and effectiveness of four architectures of Recurrent Neural Networks being respectively: GRU, BiGRU, LSTM, and BiLSTM, and tests their suitability for the PV power forecasts.

Table 1. Summary of recent approaches, their specifications, and main contributions

Ref.	**Specification**			**Main contribution**
	Location	**PV capacity**	**Horizon**	
Geng et al., 2023	China	211.37 kW Data (7 years)	1 h	Incorporates a hybrid Time2Vec - WDCNN-BiLSTM
Feroz Mirza, et al., 2023	China	Data (1year)	15min	Addresses the gradient vanishing issues using sing hybrid methods.
Wang et al., 2020	USA	Data (6years)	24h	Applies a TCM and PDPP to adjust the output of LSTM-RNN
Mansoor et al., 2023	Malaysia	Data (2 years)	15min	Proposes two new hybrid models resulting a higher convergence rate and lower stochastic error.
	Turkey	Data (2 years)	15min	
Hassan et al., 2021	Algeria	20 MW Data (2 years)	15 to 60min	Implement a NARX model and utilized a genetic algorithm for gradient-free training.
Keddouda et al., 2023	Algeria	PVc :160 W	3 s	Explores the utilization of a FFNN with RPL and PL.
Khelifi et al., 2023	Algeria	135.1 MW	30min	Analyzes the implementation of a TVF-EMD with ELM.
Guermoui et al., 2021	Algeria	73MW Data (2 years)	15 to 60min	Conceives a model ELM based model integrated with Recursive Intrinsic Functions decomposition for feature extraction
	Australia	5.04kW Data (2 years)		
Ziane et al., 2021	Algeria	6 MW Data (1year)	--	Examines the correlation between meteorological variables and photovoltaic output.
Dairi et al., 2020	Algeria	9 MW	15 to 60min	Underscores the VAE's ability to learn high-level features that enhance forecasting accuracy.
Harrou et al. 2020	Algeria	9 MWp Data (1year)	15min	Investigates LSTM's effectiveness in handling data dependencies.
Zafar et al., 2022	Turkey	Data (1year)	24h	Proposes an improvised dynamic group-based cooperative search mechanism with RBNN.
Sahin et al., 2023	Marocco	500 kWp	Short term	Uses PCA to reduce PV feature dimensions.
Thaker & Höller, 2024	Australia	8910 Wp	1 to 6 h	Provides a detailed analysis of deterministic and probabilistic forecasting model
Our paperA	Algeria	53MW	3h	Temporal insights through monthly variability assessment

By addressing these research gaps and employing a comprehensive approach, this study aims to significantly enhance the accuracy and applicability of PV power forecasting models, thereby contributing to the advancement of photovoltaic energy integration within the broader renewable energy field. The remainder of the paper is structured as follows: Section 3 provides an overview of the PV farm and outlines the fundamentals of Recurrent Neural Networks (RNNs). Section 4 details the methodology, including data pre-processing and simulation procedures. Finally, Section 5 presents the results, discussions, and concluding insights.

3. MATERIAL AND METHODS

3.1 Introduction to the PV farm

The photovoltaic field depicted in Figure (2) is a utility-scale power plant with a capacity of 53MW, which is integrated into the high-voltage grid operating at 60kV. The PV station under study is located in Ain El Bell, a southern Algerian region. This area is notable for its significant solar photovoltaic potential, as illustrated in Figure (3).

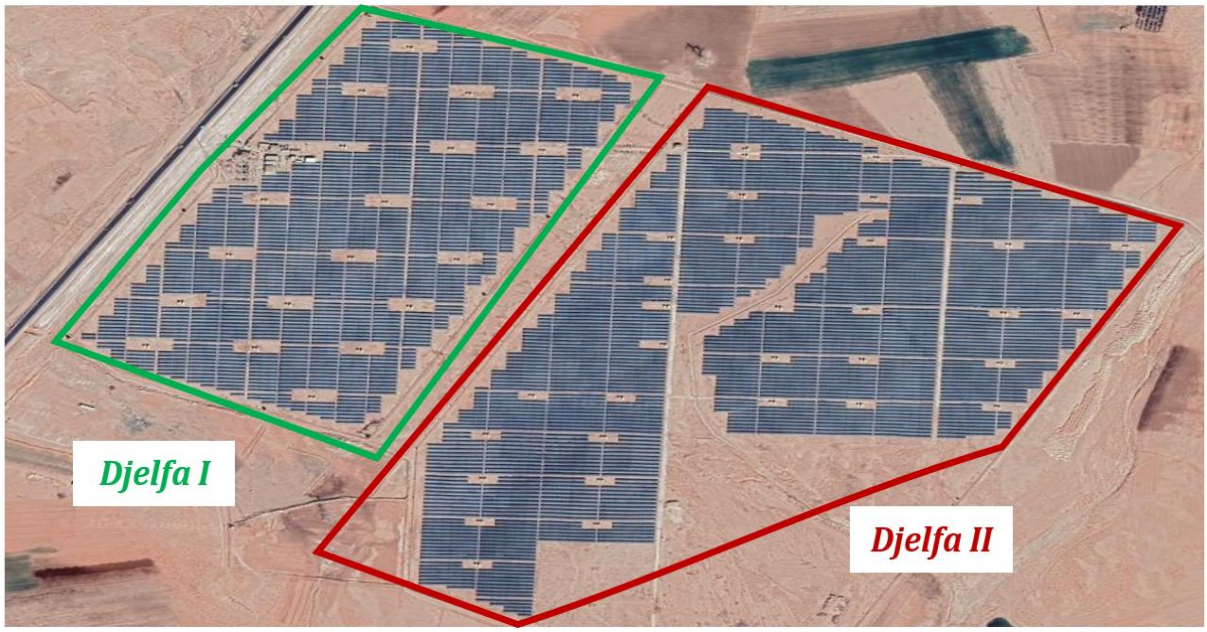

Fig 2. Djelfa photovoltaic power plant

The US PVPP comprises 212212 panels, specifically YL250P-29b polycrystalline modules, securely mounted on ground-mounted structures at a tilt angle of 33° facing south to optimize sunlight exposure and enhance energy conversion efficiency. These PV modules are divided into 53 sub-fields, each approximately 1 MWp in size, containing 4004 photovoltaic modules, 182 strings, and 91 supporting structures, with each string accommodating 22 modules.

Eight strings are connected in parallel via a combiner box, and subsequently, every three combiner boxes are arranged in parallel within the DC power distribution box. This configuration necessitates the utilization of 24 combiner boxes and 8 DC power distribution boxes for every 1 MW of power generated. An illustration depicting a sub-field unit is presented in Figure (4) for reference.

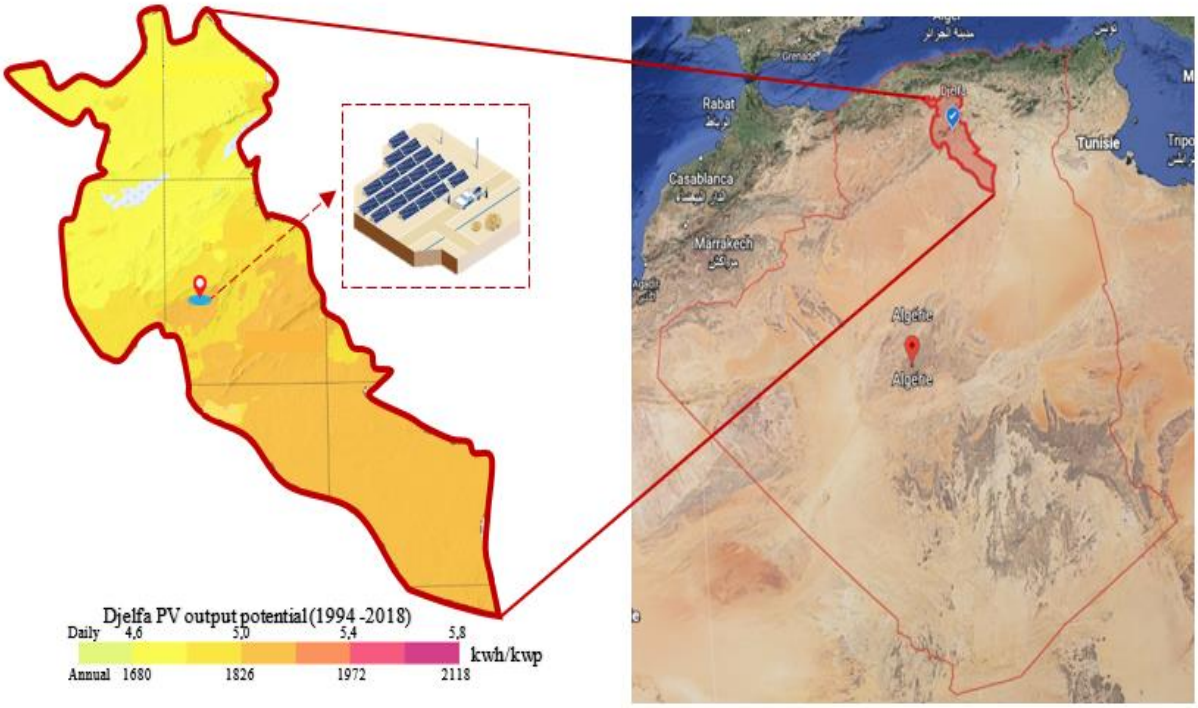

Fig 3. Annual and daily averages of photovoltaic output potential calculated from 25 recent years historical data (1994 -2018)

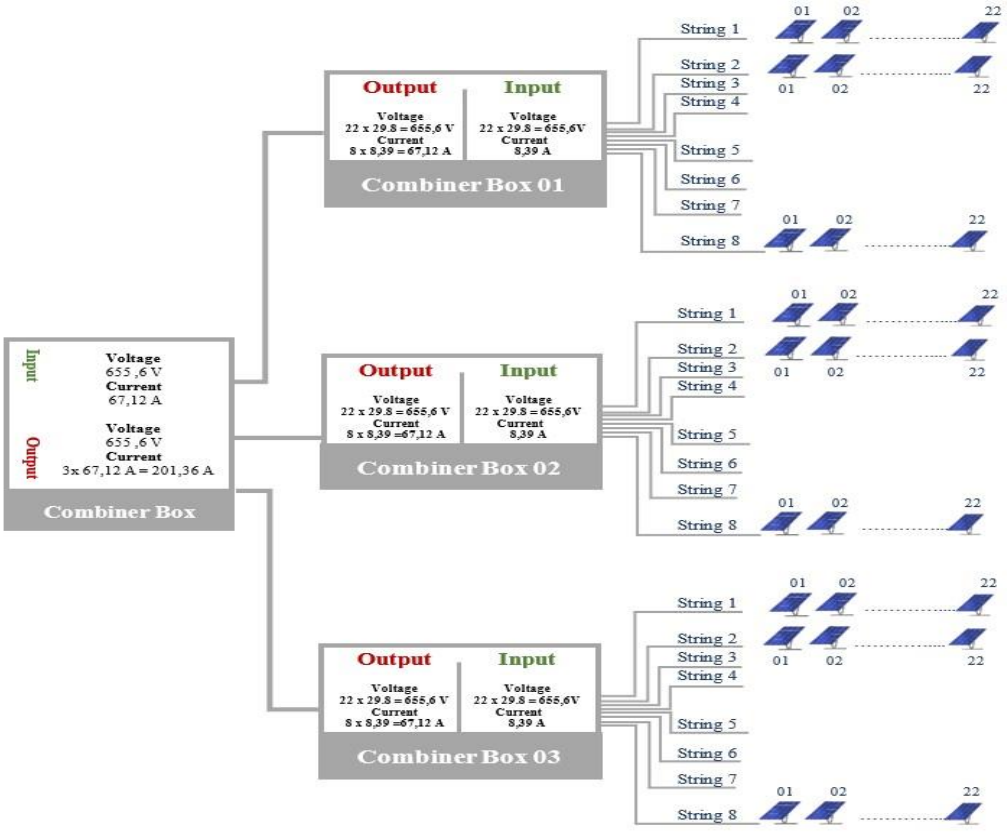

Fig 4. Schematic overview of a 1 MW subfield located in Djelfa PV plant

In addition to the photovoltaic generator, the power station is equipped with 53 inverters and 53 main transformers. The main transformers serve to elevate the voltage to 30kV. These three-phase systems are housed within SafeRing-36kV cells, which function as ring main units (RMUs), facilitating the connection of the transformer to the preceding and the onward sub-field transformers. Within this station, every ten sub-field transformers are interconnected, forming a loop through the utilization of SafeRing-36kV devices. The terminals, serving as the starting and ending points, of each loop, are directed towards the low-voltage cells positioned at the discharge point. One notable advantage of this loop configuration is the reduction in the number of output cables and their associated costs. Additionally, it provides an alternative energy supply in the event of issues occurring within one of the sub-fields, ensuring uninterrupted service continuity.

At the discharge point, the electricity is further elevated to 60kV using a secondary transformer before being injected into the power grid. The discharge point also serves as the interface between the power plant and the external power grid, enabling it to connect or disconnect the photovoltaic station from the electrical grid, supply power to auxiliary systems, facilitate electricity metering through voltage and current transformers, promptly interrupt the connection with the network to ensure the safety of both the plant and the network in the event of electrical equipment failure. Figure (5) illustrates the USPVPP main components.

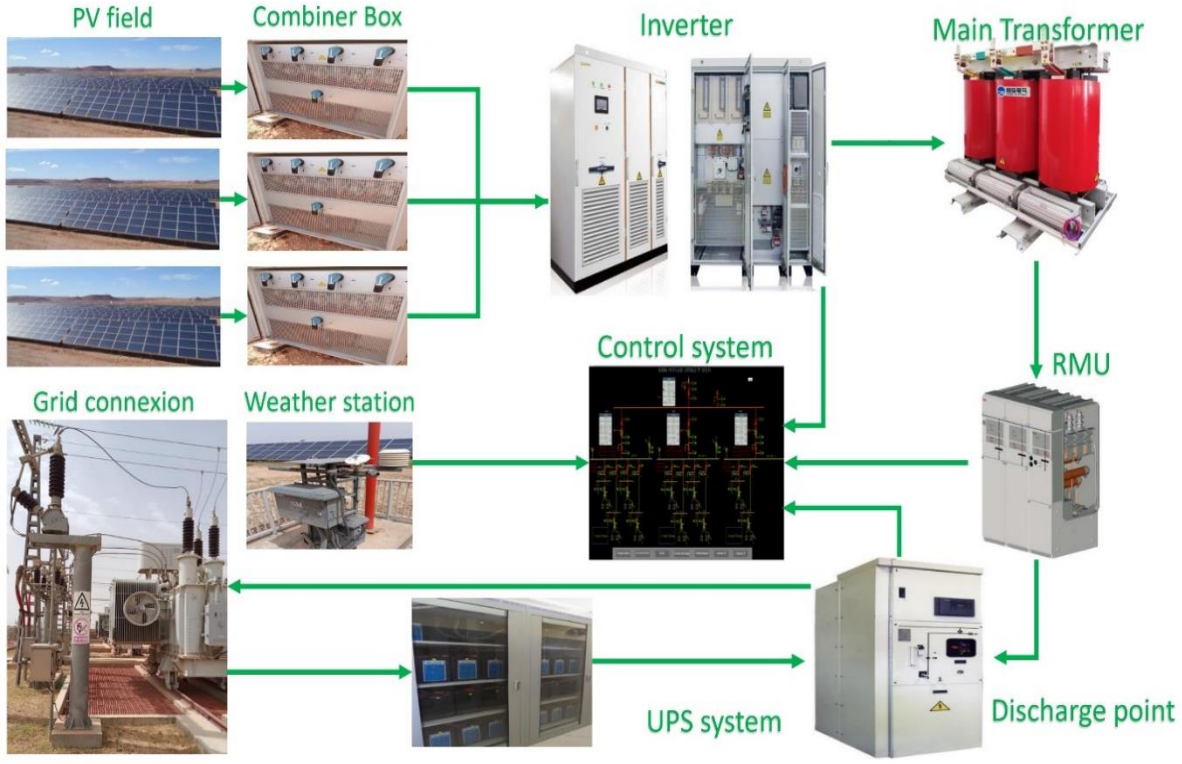

Fig 5. Schematic diagram of the 53MW Djelfa solar power plan

Throughout the year, the PV power energy fluctuates due to solar radiation variations. These divergences are primarily influenced by the Earth's elliptical trajectory encircling the Sun, which changes the distance between the Earth and the Sun, and thereby the tilt of the Sun's rays, known as the solar incidence angle. This variation impacts the intensity of solar radiation received and thereby the potential of PV generation. Figure (6) offer a graphical analysis of the generated power for the studied PV farm, showing various values produced over the months, with the Spring season remaining the best season for

the studied PV farm as the maximum produced PV according to the recordings is attained on February, ten at 14h:00 (maxP_{max} = 58.34 MW). Moreover, the maximum value of Pmax is recorded during March (meanP_{max} = 46.42 MW). While a decline in maximum production is registered during warm months such as August, July, and June. Finally, the minimum value of P_{max} is obtained on November, 24th at 15h:00 (minP_{max} = 7.41 MW).

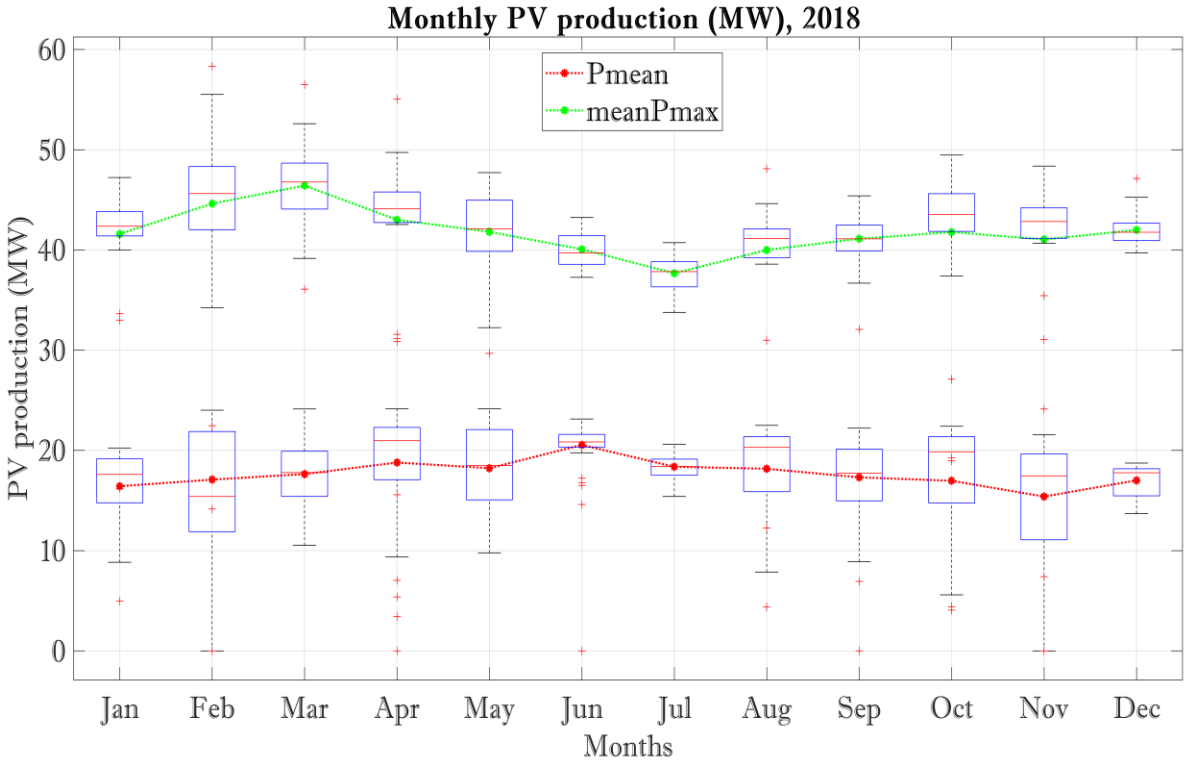

Fig 6. Monthly PV production (MW), 2018

3.2 Overview of Bidirectional RNN

3.2.1 Long Short-Term Memory

A pivotal element within LSTM is the memory cell (MC), which functions as enduring storage throughout the computational process. The MC facilitates information transfer across the entire sequence, regulating the flow based on decisions made by gate mechanisms. In contrast to traditional RNNs, LSTM excels in efficiently managing valuable information over extended durations, thereby mitigating the vanishing issues associated with conventional RNNs. (Agga et al., 2021 ; Cao et al., 2023) LSTM architecture involves adding three gate structures: input, output, and forget gates, as represented in Figure (7). Forget Gate helps to forget the redundant information and save only the relative information to proceed with prediction. (Liu et al., 2023) The input gate (i_t) is responsible for controlling the flow of new information and specifies whether and, if so, to what extent new information should be used in the current state cell (c_t). The output gate (o_t) determines how much of the information from the previous time step is transferred to the next along with the information from the current time step. (Dhaked, Dadhich, & Birla, 2023) The calculated values are in the 0 to 1 forget gate range. When the f_t is close to 1 and the i_t is close to 0, LSTM can achieve the long-term memory function; otherwise, it can realize the short-term memory function (Agga et al., 2021; Cao et al., 2023) .

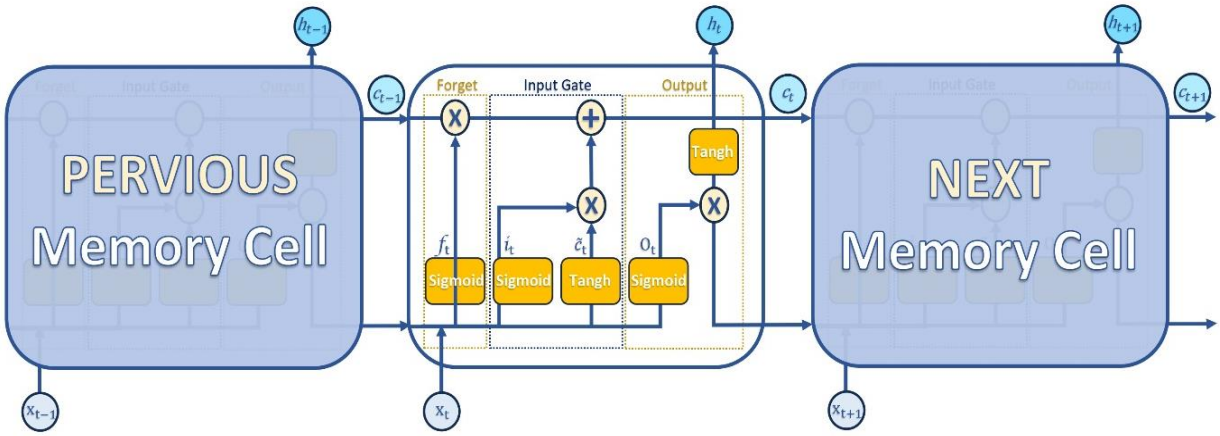

Fig 7. Basic architecture of LSTM model

The mathematical formulations used in the LSTM network are the following: (Al-Ja'afreh, Mokryani, & Amjad, 2023; Cao et al., 2023; Dhaked et al., 2023; Sadeghi et al., 2023)

- **The gate units**

$$i_t = \sigma(W_{ix}x_t + W_{ih}h_{t-1} + W_{ic}c_{t-1} + b_i) \quad (1)$$

$$f_t = \sigma\left(W_{fx}x_t + W_{fh}h_{t-1} + W_{fc}c_{t-1} + b_f\right) \quad (2)$$

$$o_t = \sigma(W_o x_t + W_{oh}h_{t-1} + W_{oc}c_{t-1} + b_o) \quad (3)$$

- **The memory unit**

$$\bar{c}_t = tanh\left(W_{\bar{c}_t}x_t + W_{\bar{c}_t h}h_{t-1} + b_g\right) \quad (4)$$

$$c_t = f_c \odot c_{t-1} + i_t \odot \bar{c}_{t-1} \quad (5)$$

- **The output unit**

$$h_t = o_t \odot tanh(c_t) \quad (6)$$

The cell state of the MC is denoted c_t , and the candidate MC is expressed as $\bar{c}_t$, where c_{t-1} represents the cell state at time t_{-1}. Additionally, x_t refers to the input components, and h_t corresponds to the hidden state. W_{ix}, W_{fx}, W_{ox}, and Wc are the weights for the i_t, f_t, o_t, and $\bar{c}_t$, respectively. W_{ih}, W_{fh}, W_{oh} , and $W_{\bar{c}_t h}$ represent the weight matrices for the hidden layers. Additionally, W_{ic}, W_{fc}, W_{oc} are weight matrices for the candidate cell state .Subsequently, b_i, b_f, b_o, and b_g stand for the bias vectors associated with the three gates and MC, respectively. The activation function utilized includes the sigmoid function (σ) and the hyperbolic tangent function (tanh). In a neural network, the activation function serves as a mathematical operation associated with a node (or neuron) that is activated when the input value of the node contributes significantly to the prediction process. Numerous types of activation functions exist, with the sigmoid, hyperbolic tangent, and logistic functions being widely utilized. (Mamdouh, Ezzat, & Hefny, 2024).

3.2.2 Gated Recurrent Unit

In comparison to the LSTM's three-gate configuration, the GRU integrates the forget gate and the input gate into a singular update gate. Thus, the GRU consists exclusively of an update gate and a reset gate. the reset gate determines how much of the previous hidden state to forget, and the update gate determines how much of the new input information to incorporate into the hidden state. The hidden state is then updated based on the values of the reset and update gates, as well as the new input. The proposed GRU structure not only speeds up the convergence rate but also avoids the gradient problems in RNN. (Wu et al., 2024) The internal structure of the GRU is shown in Figure (8).

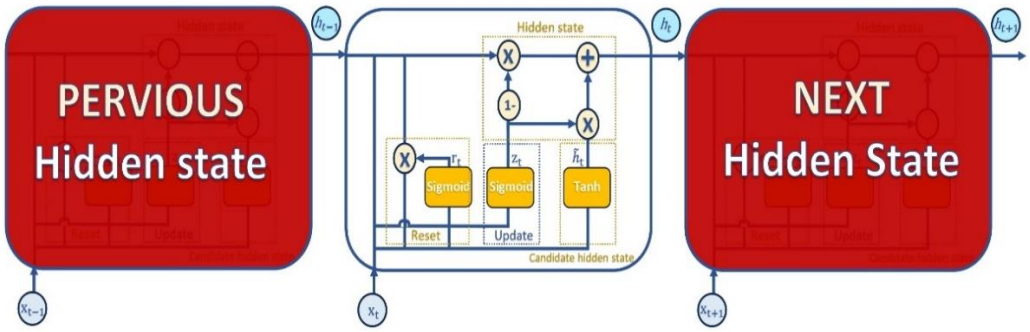

Fig 8. The basic architecture of the GRU model

The GRU presents a simpler internal structure than the LSTM. Where h_{t-1} is the state transmitted from the previous one, x_t denotes the input of the current node, h_t signifies the output of the hidden layer, r_t is the reset gate, z_t represents the update gate, $\tilde{h}_t$ is the candidate's hidden state, and 1- symbolizes the data transmitted forward by the link as $1-z_t$. The sigmoid function facilitates the transformation of data into a range between 0 and 1, thereby serving as a gating mechanism. As r_t approaches zero, the model selectively retains only the current input information while discarding previously held hidden information. Conversely, as r_t approaches 1, the model preserves historical information. The value of z_t varies from 0 to 1; higher values of the gated signal imply greater retention of information. The units derived from GRU can be computed using the following equations (Wu et al., 2024):

- **Reset gate:**

$$r_t = \sigma(W_{rx}x_t + W_{rh}h_{t-1} + b_r) \tag{7}$$

- **Update gate:**

$$z_t = \sigma(W_{zx}x_t + W_{zh}h_{t-1} + b_z) \tag{8}$$

- **Candidate hidden state:**

$$\tilde{h}_t = tanh(W_{hx}x_t + r_t \odot (W_{hh}h_{t-1}) + b_h) \tag{9}$$

- **New hidden state:**

$$h_t = (1 - z_t) \odot h_{t-1} + z_t \odot \tilde{h}_t \tag{10}$$

3.2.3 Bidirectional Recurrent Networks

When employing time series data for PV power forecasting, meticulous consideration of the influence of past and future values on the current value is imperative to attain precise estimations. Consequently, establishing forward and reverse Recurrent Neural Network (RNN) models is conducive to comprehending the intricate relationship between preceding and subsequent factors that impact prediction outcomes. A Bidirectional Recurrent Neural Network (BiRNN), exemplified by BiLSTM or BiGRU, features two hidden layers interconnected in opposing directions, yielding a singular output. Data is ingested in two temporal directions: one adhering to the conventional time sequence and the other in reverse temporal order. This dual-directional approach facilitates the incorporation of insights from both antecedent and subsequent instances at each time step. It is noteworthy that bidirectional neurons operate autonomously during forward and backward passes, with only the weights undergoing adjustment during training. The architectural frameworks of both BiGRU and BiLSTM are delineated in Figure (9) and Figure (10), respectively.

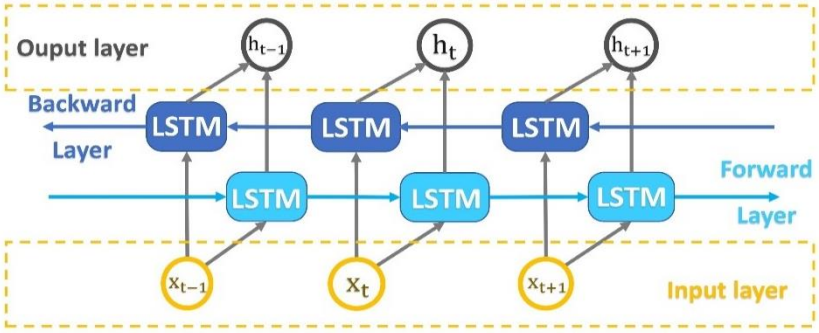

Fig 9. Circular Architecture of Bidirectional LSTM

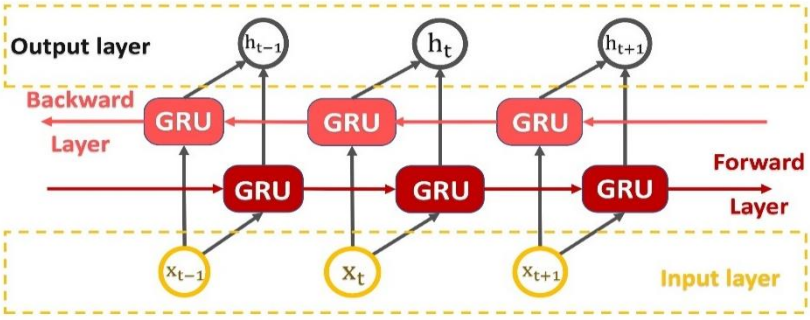

Fig 10. Circular Architecture of Bidirectional GRU

$\{x_{t-1}, x_t, xt_{+1} \ldots x_n\}$ are the signal's input, whereas $\{h_{t-1}, h_t, h_{t+1} \ldots h_n\}$ denotes the network's output. To compute y_t prediction at time t, the following activation function is used (Mamdouh et al., 2024):

$$y_t = f(W_y[\overrightarrow{h_t}; \overleftarrow{h_t}] + b_y) \quad (11)$$

W_y : is the network's final transformation weight based on the input and volume set. $\overrightarrow{h_t}$ is the forward hidden state at time t. $\overleftarrow{h_t}$ is the backward hidden state at time t. $[\overrightarrow{h_t}; \overleftarrow{h_t}]$denotes the concatenated hidden states from both the forward and backward directions. b_y the bias vector associated with the final transformation layer.

Another pivotal consideration lies in the applicability of the Bidirectional technique for long-term PV power prediction. Forecasts for PV power frequently span hours, if not days, making the method's adeptness in capturing extended dependencies exceedingly valuable. By accounting for both past and future time increments, the model produces dependable forecasts for extended durations. The Bidirectional mechanism empowers the model to grasp temporal trends, manage periodicity, depict time-based correlations, and enable precise long-term predictions. Integration of these temporal features notably augments the precision and dependability of PV power prediction, thereby fostering progress within the domain (Feroz Mirza et al., 2023).

3.3 Forecasting methodology

The objective of this research is to examine the monthly performance patterns of four predictive models tailored for forecasting three hours ahead of PV power generation. These models include various architectures of Recurrent Neural Networks: Long Short-Term Memory (LSTM), Bidirectional Long Short-Term Memory (Bi-LSTM), Gated Recurrent Unit (GRU), and Bidirectional GRU (Bi-GRU). By scrutinizing the statistical indicators across different months, this study elucidates the comparative strengths and weaknesses of these models in the forecasting domain. As depicted in Figure (11), our methodology involves collecting data from multiple PV technologies, pre-processing this data to ensure its suitability for analysis, training and optimizing the four algorithms, validating their performance across different metrics, identifying seasonal patterns, and finally selecting the most suitable predictive model for the studied region.

This comprehensive approach aims to determine the adaptability and accuracy of the four architectures of RNN in forecasting the PV output under varying conditions. The detailed steps of the proposed study's methodology are as follows:

- **Data Collection and Enhancement:** The initial phase of the study is focused on detailed data collection and comprehensive processing. Essential activities in this stage encompass rectifying missing values, identifying and removing anomalies, and excluding non-essential night-time data.
- **Data Splitting Strategy:** The dataset is strategically divided into training and testing segments. 50% of the data is allocated for training, while the remaining 50% is reserved for testing. This ratio is kept constant through all simulations.
- **Optimizing the LSTM, BiLSTM, GRU, and BiGRU Models:** In this stage, the deep LSTM model undergoes a rigorous tuning process through grid search methodology. This process is aimed at identifying the most effective hyper-parameters, ensuring the model's ability to deliver precise and reliable PV power forecasts.
- **Analysis and Performance Metrics Assessment:** Additional steps include conducting a comparative analysis of the model's forecasts against actual data, and evaluating its performance using a range of metrics such as RMSE, MAE, and others. This analysis is crucial in understanding the model's strengths and limitations in real-world scenarios.
- **Seasonal Patterns:** The next step is to delve deeper into understanding the model's patterns within the data, particularly during specific times of the year, and to analyze their seasonal variations. This involves not only recognizing recurring trends but also identifying the underlying factors driving these fluctuations across different seasons. By doing so, we can gain a more comprehensive understanding of how the model interacts with the data over time and refine our insights accordingly.

- **Model Comparison and Selection:** When comparing performance metrics across different RNN architectures, one can assess which model outperforms others either comprehensively or in specific months. This rigorous comparison, supported by thorough data analysis, serves as a compass for selecting the most appropriate model tailored to the prediction task and its time duration. By scrutinizing performance variations over time, we gain insights into each model's strengths and weaknesses, enabling informed decisions about which architecture is most adept at capturing the nuances of the data across various temporal scales.

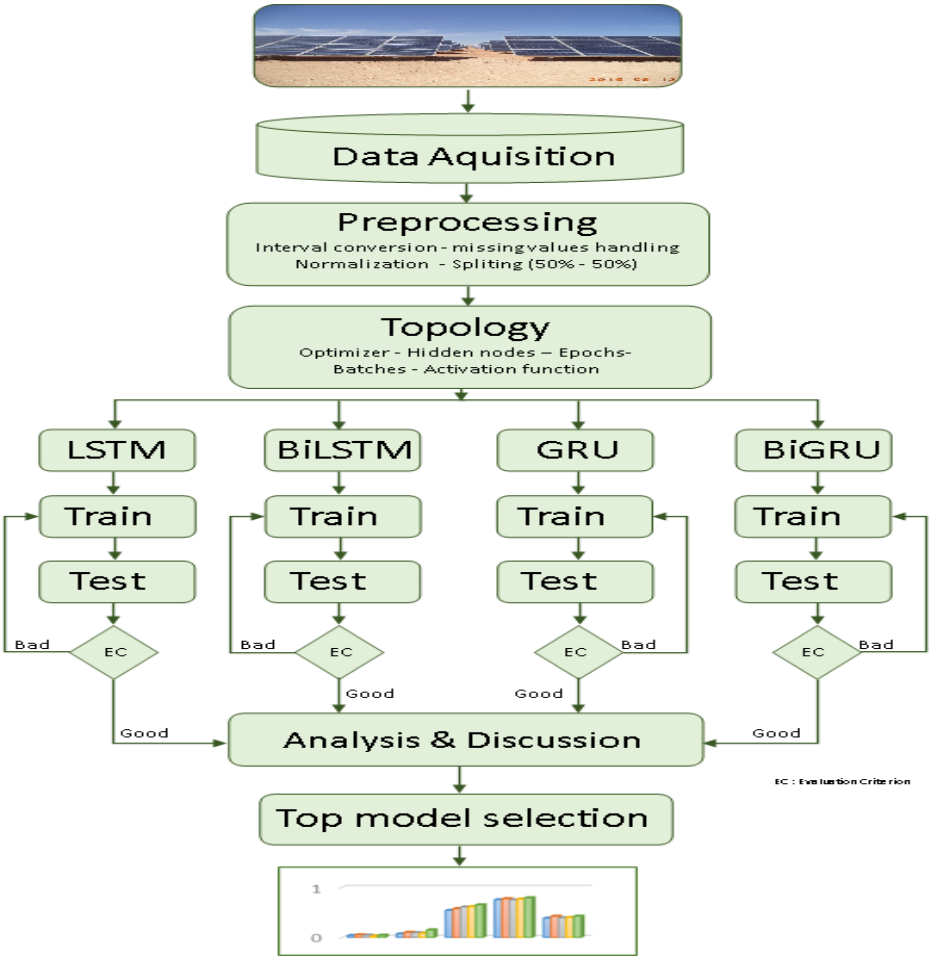

Fig 11. Flowchart of the investigation methodology

3.4 Data acquisition and preprocessing

The Ain El Bell weather station operates as a fully automated system, consisting of four primary components: the sensor module, communication module, data acquisition module, and power supply module (refer to Figure 12). The sensor module includes multiple weather sensors, each designed to capture specific climate parameters. Once data is collected, the acquisition system processes the signals; converting analog inputs to digital formats for statistical analysis. The processed data is then transmitted to the control center through the communication module. Meanwhile, the power module ensures a continuous energy supply, enabling the seamless operation of all components.

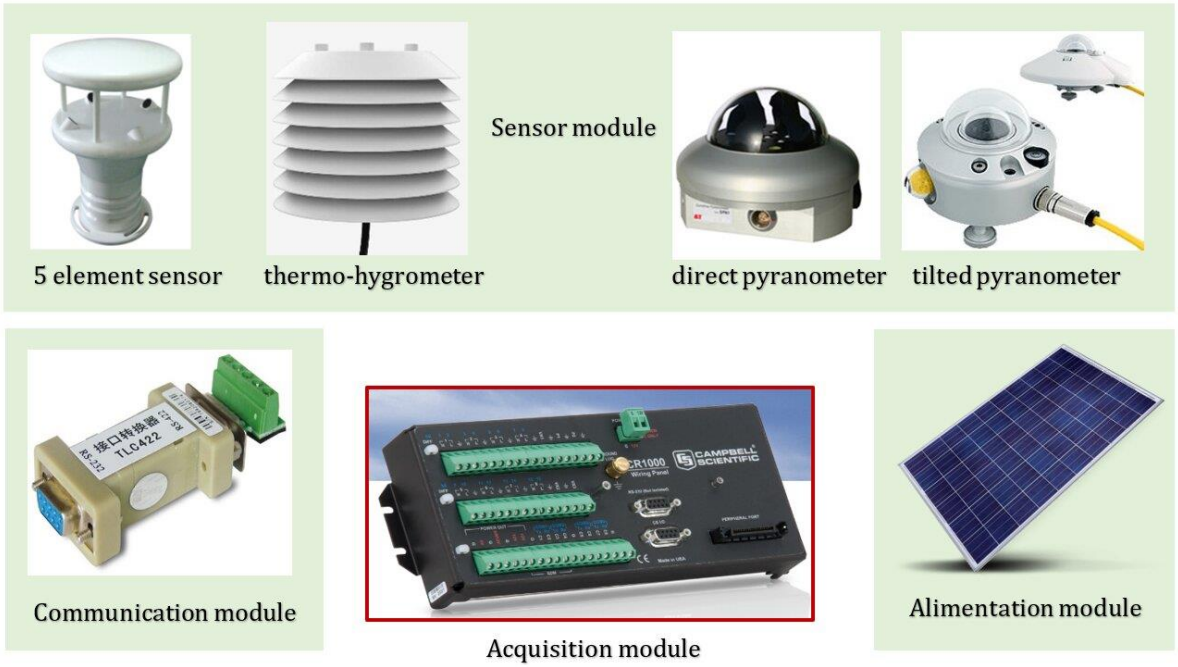

Fig 12. Photovoltaic automatic weather station modules

In this study, we utilize a dataset comprising 21046 measurements of PV generation data. These measurements span from the early morning at 6 a.m. to evening at 8 p.m., with readings taken at 30-minute intervals. While the intraday forecast horizon is crucially supported by power supply systems, The data's temporal resolution has been converted from 30-minute intervals to 3-hour intervals using a programmed algorithm that calculates averages across five specified time periods (6:00 AM - 9:00 AM, 9:00 AM - 12:00 PM, 12:00 PM - 3:00 PM, 3:00 PM - 6:00 PM, and 6:00 PM - 8:00 PM). This transformation effectively summarizes the dataset into 3-hour segments. We believe this adjustment enhances the practicality of evaluating the intraday potential of the PV station and facilitates more efficient grid scheduling.

In the construction of our predictive model, we allocate 50% of the entire dataset for the training phase, ensuring ample data to learn the underlying patterns and dynamics. The remaining 50% is reserved for testing purposes, allowing us to evaluate the model's performance on unseen data and assess its generalization ability. This balanced approach helps ensure the reliability and robustness of our model in real-world applications.

Additionally, bias can arise in the developed model, especially when various types of data (with different units) are used, leading to different ranges of variation, such as Temperature (°C), PV power (MW), and Global solar radiation (Wh.m^{-2}). Additionally, outliers may manifest within the dataset. Normalizing the data serves to align all features onto a comparable scale, thereby mitigating the influence of outlier data by assimilating them within the range of other data points. Various normalization techniques are available. In our study, we employ Min-Max normalization, delineated in equation (12) as follows (Sadeghi et al., 2023):

$$\bar{X}_i = \frac{X_i - X_{min}}{X_{max} - X_{min}} \tag{12}$$

$\bar{X}_i$: Is the normalized data
X_i : Is the original data
X_{min} , X_{max} : are minimal and maximal values contained in the dataset.

3.5 Simulation details

3.5.1 Hardware and software requirements.

The two models are developed using the Python 3.11. language within the Visual Studio environment. All simulations are executed on a computer equipped with a 64-bit operating system, 16.00 GB of RAM, and an Intel(R) Core (TM) i7-9850H CPU @ 2.60GHz.

3.5.2 Model parameters

Generally, a model's precision is affected by several factors such as the training data volume, network architecture, hyperparameters, and optimization techniques used for weight and bias adjustment. (Al-Ja'afreh et al., 2023; Dhaked et al., 2023). Nonetheless, to assess the monthly behavior of the developed models, the parameters listed in Table (2) remained consistent across all processes.

Table 2. Main parameters of the models

Activation function	Tangent Hyperbolic
Optimization algorithm	Adam
Number of hidden nodes	50
Maximum number of training epochs	100
Mini-batches used during training	32

3.6 Evaluation criterion

To assess the results, several metrics are employed (ElRobrini et al., 2024), including the Mean Absolute Error (MAE), Mean Square Error (MSE), normalized Root Mean Square Error and (nRMSE), and the coefficient of determination (R^2), whose mathematical expressions are given by:

$$R^2\ (\%) = 1 - \frac{\sum_{i=1}^{n}\left(I_{i,measured} - I_{i,predicted}\right)^2}{\sum_{i=1}^{n}\left(I_{i\ ,measured} - \hat{I}_{i,measured}\right)^2} \tag{13}$$

$$MAE = \frac{1}{n}\sum_{i=1}^{n}\left|I_{i,predicted} - I_{i,measured}\right| \tag{14}$$

$$MSE = \frac{\sum_{i=1}^{n}(I_{i,predicted} - I_{i,measured})^2}{N} \tag{15}$$

$$nRMSE(\%) = \frac{RMSE}{Max(I_{measured}) - Min(I_{measured})} * 100 \tag{16}$$

4. RESULTS AND DISCUSSIONS

Utilizing the eight most recent historical inputs (a delay of 8 last values), the training of the four recurrent neural network architectures - LSTM, BiLSTM, BiGRU, and GRU- was conducted. Their performances

were evaluated using metrics including R-squared values, Normalized Mean Absolute Error, Mean Squared Error, and Root Mean Squared Error. LSTM demonstrates commendable performance overall, with R-squared values ranging from approximately 0.647 to 0.901, albeit with some variance across months. BiLSTM generally outperforms LSTM, consistently yielding higher R-squared values ranging from around 0.744 to 0.934, and displaying less variability throughout the year. Similarly, GRU exhibits good R-squared values ranging from about 0.800 to 0.945, with slight fluctuations across months. However, the most notable performance is seen in BiGRU, particularly evident in November and December. BiGRU showcases superior performance compared to the other models, maintaining consistent and robust performance throughout the year, with R-squared values ranging from approximately 0.814 to 0.943. November and December are consistently identified as the most challenging months for prediction across all models, possibly due to seasonal changes and irregular patterns specific to those months. Remarkably, Bidirectional GRU delivers noteworthy results despite the challenges posed by the autumn and winter months, demonstrating its resilience in handling complex temporal data and effectiveness in capturing underlying patterns. Conversely, June, July, and October emerge as the months with the Best R-squared scores. The results are displayed in Figure (13).

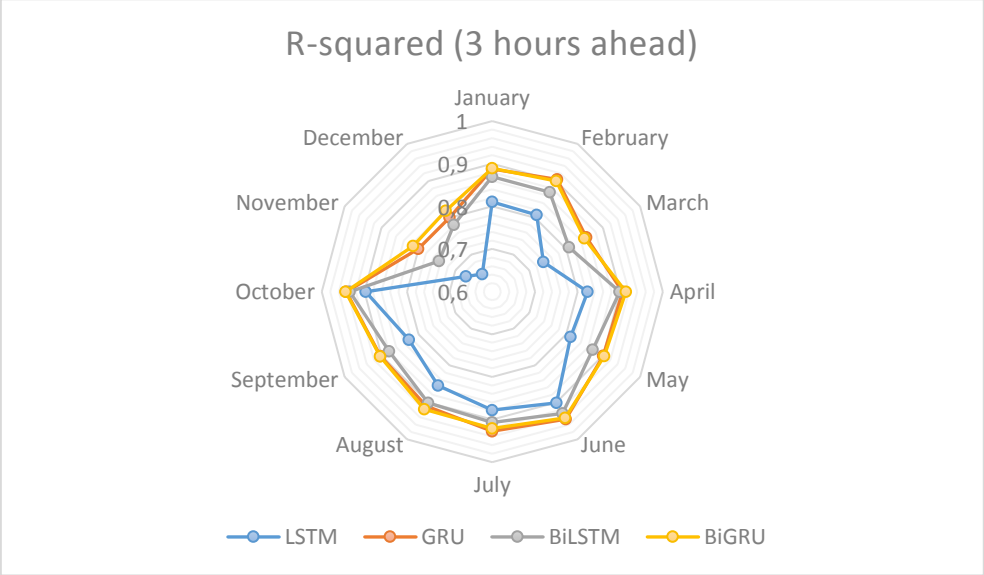

Fig 13. Monthly R-squared values

Based on the calculated NRMSE values for each month, many observations were noted. For example, in January, BiGRU performed the best with an NRMSE of 11.2%, followed closely by LSTM and BiLSTM, while GRU had a slightly higher NRMSE. From February to May, BiGRU consistently maintained the lowest NRMSE values among all models, indicating better predictive accuracy during these months. In June and July, all models showed lower NRMSE values compared to previous months, but BiGRU remained the best-performing model. From August to October, all models had relatively low NRMSE values, with BiGRU consistently performing the best. In November and December, there was a noticeable increase in NRMSE values for all models as depicted in Figures (14) and (15), suggesting challenges in prediction during these months. However, BiGRU still maintained the lowest NRMSE compared to other models. Overall, the NRMSE values suggest that BiGRU consistently outperformed LSTM, GRU, and BiLSTM across most months, indicating its superior predictive accuracy. Therefore, BiGRU appears to be the most suitable model for forecasting the PV power plant for this station (Djelfa I and II).

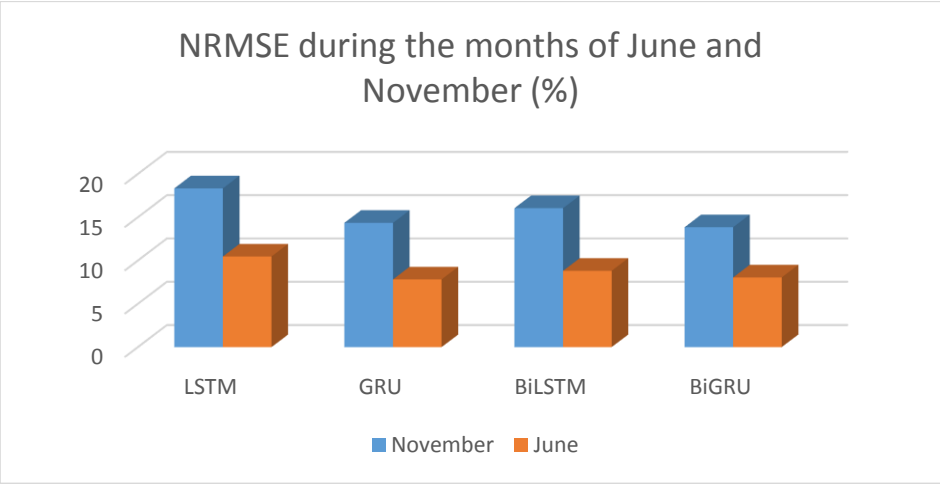

Fig 14. The variability of NRMSE during June and November

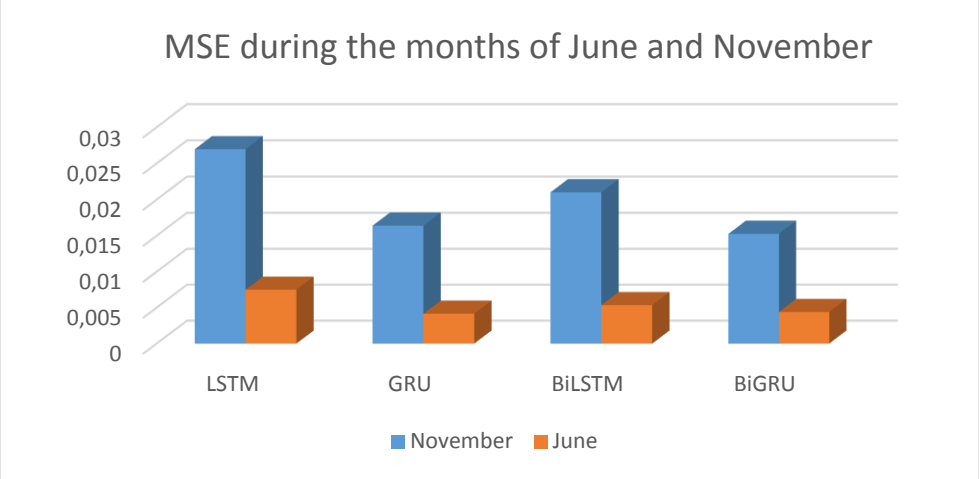

Fig 15. The variability of MSE during June and November

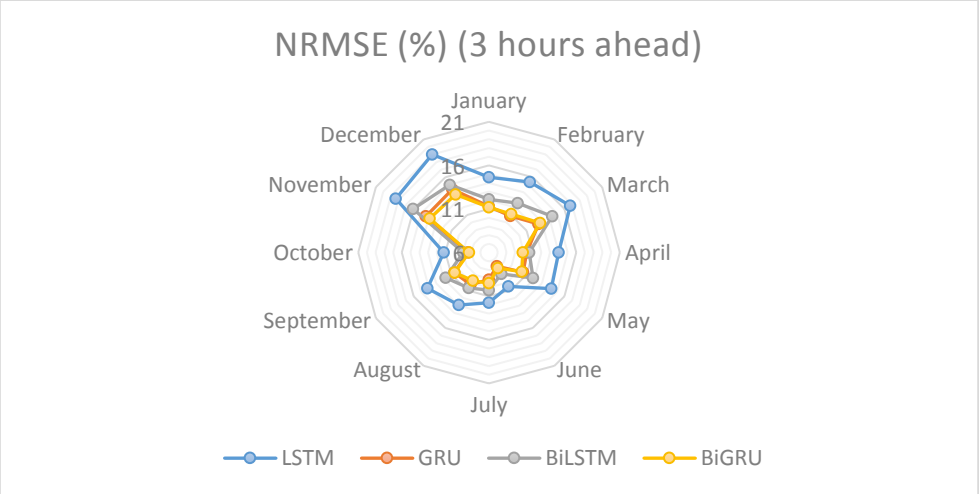

Fig 16. Monthly NRMSE values

Moving to Mean squared Errors, all models exhibit lower values in the middle months of the year (June to September), ranging from approximately 0.0042 to 0.0145, indicating better performance during this

period. November and December show higher MSE values across all models, ranging from approximately 0.0144 to 0.0281, highlighting the challenges in prediction during these months. Bidirectional GRU tends to have the lowest MSE values in most months, ranging from approximately 0.0044 to 0.0153, indicating better overall predictive accuracy compared to LSTM, GRU, and BiLSTM. A comparison between the mean square error (MSE) during November and June is depicted in Figure (16), whereas the comprehensive findings are depicted in Figure (17).

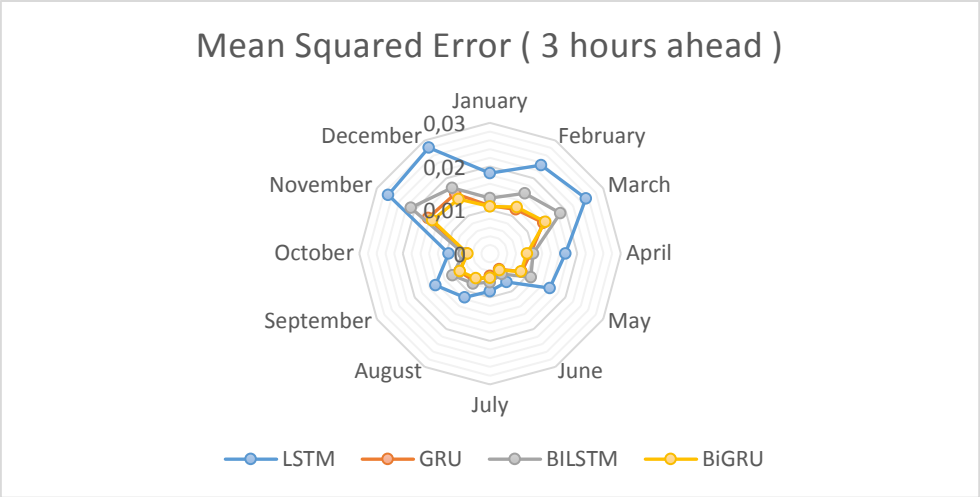

Fig 17. Monthly variation of MSE

The Mean Absolute Error in Figure (18) exhibits similar trends as those observed in MAE and NRMSE. All models exhibit higher MAE values in the winter months (November and December) and lower MAE values in the summer months (June to August), supporting the seasonal patterns in predictive accuracy. There is variability in MAE values across different months for all models, but BiGRU generally shows more consistent performance, with relatively lower MAE values across months compared to LSTM, GRU, and BiLSTM.

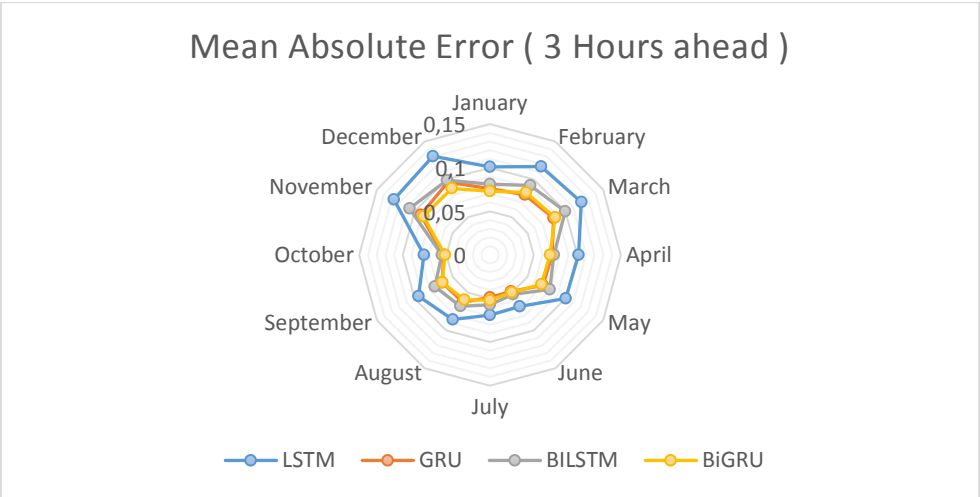

Fig 18. Monthly variation of MAE

The histograms presented in Figure (19) showcase the performance of the four architectures across intraday intervals during the day of June. Across these intervals, the models exhibit distinct behaviors, with some consistently outperforming others. Particularly, the BiLSTM and BiGRU models tend to demonstrate superior performance compared to the LSTM and GRU models, indicating the effectiveness

of bidirectional architectures in capturing temporal patterns. The LSTM model exhibits relatively low errors during the early morning (6h-9h) and late evening (18h-20h) intervals. However, it struggles more during the midday intervals. The GRU model shows comparable performance to the LSTM model, with relatively low errors during the early morning and late evening intervals, and slightly higher errors during the midday intervals (12h-15h). The BiLSTM model generally performs slightly better than the LSTM model, with slightly lower errors across all time intervals. The BiGRU model appears to perform the best among the four models, with consistently lower errors across all time intervals compared to both the unidirectional LSTM and GRU models.

Interestingly, this trend is not consistent when exploring a day in November (Figure (20)). For the LSTM model, we observe varying levels of error across different time intervals. The highest error occurs during the 6h-9h and 15h-18h intervals, suggesting difficulty in accurately predicting values during these periods. Conversely, the lowest error is recorded during the 18h-20h interval. The GRU model exhibits fluctuations in error rates across the time intervals. Notably, it demonstrates relatively low errors during the 9h-12h and 15h-18h intervals, while the highest error occurs during the 6h-9h interval. Moving to the bidirectional architectures, both BiLSTM and BiGRU models showcase improvements over their unidirectional counterparts in capturing temporal patterns. BiLSTM performs particularly well during the 9h-12h interval, while BiGRU excels during the 18h-20h interval. Comparing the models against the actual values reveals that all models struggle to precisely predict the target values. However, the bidirectional models generally exhibit better performance overall.

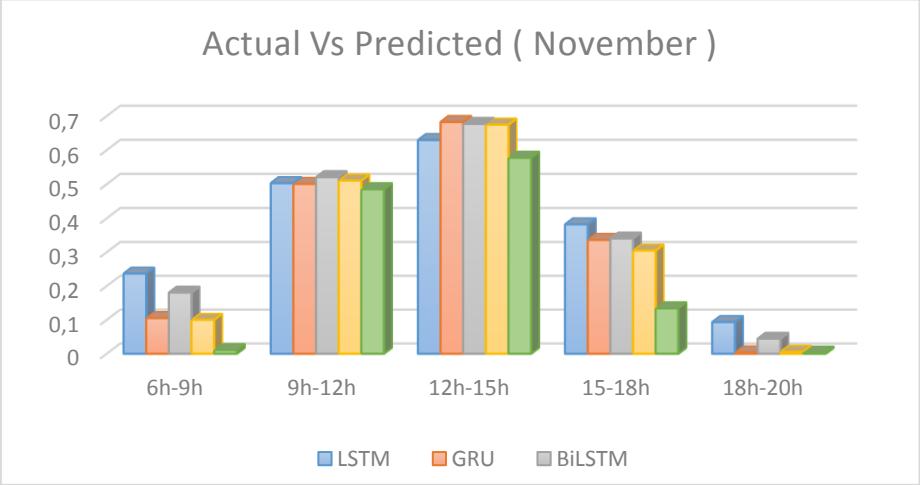

Fig 19. Predicted Vs Actual results (A Day of November)

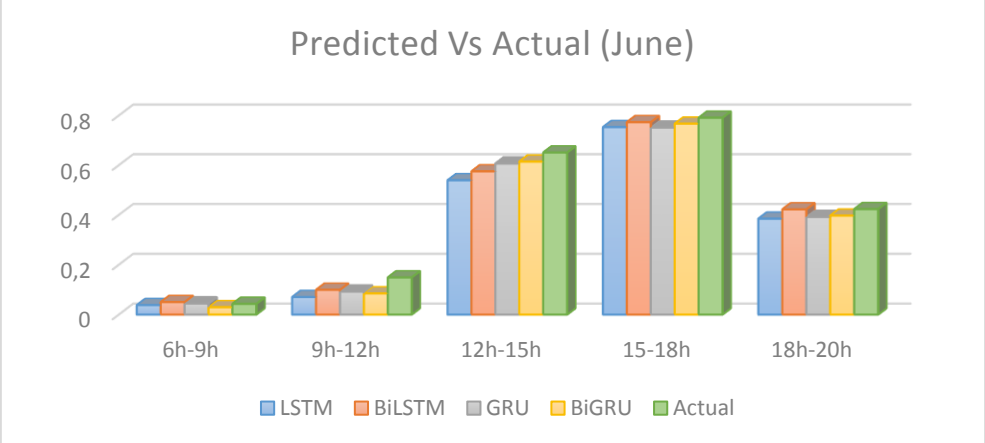

Fig 20. Predicted Vs Actual results (A Day of June)

Based on these two samples, we can conclude that the models' performance varies throughout the day across different time intervals, as well as throughout the seasons across different patterns. This indicates potential complexities in the underlying data sequences, mainly caused by their exceptional properties, features, and trends, providing insights for scrutiny of data exploration and assessment, to optimize the selection of the predictive model.

Discussions

The analysis of MAE, MSE, NRMSE, and R-squared values across different months provides insights into the performance of LSTM, GRU, BiLSTM, and BiGRU. The general ideas extracted are as follows:

- **Seasonal Patterns:** All models exhibit seasonal patterns in their performance metrics, with the worst values observed in the winter months (November and December) and pertinent values in the summer months (June to August). This suggests that the models may struggle to capture the underlying patterns in the data during certain times of the year, potentially due to factors such as increased volatility or changing dynamics.
- **Model Performance:** BiGRU consistently demonstrates better values compared to LSTM, GRU, and BiLSTM across most months. This indicates better overall predictive accuracy for BiGRU, suggesting its effectiveness in capturing complex patterns in the data and making accurate forecasts. Bidirectional-GRU's more consistent performance across different months further supports its suitability for the PV power forecasts.
- **Data Analysis Requirement:** The models exhibit varying performance patterns throughout the day across different time intervals and also demonstrate fluctuations throughout the seasons, each revealing distinct trends. These observations hint at underlying complexities within the data sequences, stemming from their exceptional properties, features, and trends. Such insights emphasize the necessity for meticulous scrutiny and comprehensive data exploration, aimed at optimizing the selection process for predictive models.
- **Model Comparison and Selection:** When comparing performance metrics across different RNN architectures, one can evaluate which model performs better overall or in specific months. This comparison, backed by Data Analysis, will guide the selection of the most suitable model for the prediction task and duration.

5. CONCLUSION

This study aims to investigate the monthly behavior of four predictive models designed for a three-hour ahead forecast horizon. The four models are Recurrent Neural Networks with different architectures: Long Short-Term Memory (LSTM), Bidirectional Long Short-Term Memory (Bi-LSTM), Gated Recurrent Unit (GRU), and Bidirectional GRU (Bi-GRU). The analysis of the statistical indicator values over the months highlights the strengths and weaknesses of these models for the forecasting task. All models exhibit seasonal patterns and variability in their performance metrics, with the lowest values observed in the winter months (November and December) and notable values in the summer months (June to August). Bi-GRU emerges as the most robust performer, with consistently lower MAE, MSE, and NRMSE values, and higher R-squared observed across different months. Therefore, based on the analysis, Bi-GRU appears to be the preferred choice for the forecasting application in this case due to its superior predictive accuracy. Another important consideration is the variation in daily performance throughout the seasons, which reveals distinct trends. These observations hint at underlying complexities within the data sequences, stemming from their exceptional properties, features, and

trends. Such insights underscore the necessity for meticulous scrutiny and comprehensive data exploration, aimed at optimizing the selection process for predictive models.

REFERENCES

Agga, A., Abbou, A., Labbadi, M., & El Houm, Y. (2021). Short-term self consumption PV plant power production forecasts based on hybrid CNN-LSTM, ConvLSTM models. *Renewable Energy*, *177*, 101-112. https://doi.org/10.1016/j.renene.2021.05.095.

Al-Ja'afreh, M. A. A., Mokryani, G., & Amjad, B. (2023). An enhanced CNN-LSTM based multi-stage framework for PV and load short-term forecasting: DSO scenarios. *Energy Reports*, *10*, 1387-1408. https://doi.org/10.1016/j.egyr.2023.08.003.

Benmouiza, K., & Cheknane, A. (2013). Forecasting hourly global solar radiation using hybrid k-means and nonlinear autoregressive neural network models. *Energy Conversion and Management*, *75*, 561-569. https://doi.org/10.1016/j.enconman.2013.07.003.

Benmouiza, K., & Cheknane, A. (2019). Clustered ANFIS network using fuzzy c-means, subtractive clustering, and grid partitioning for hourly solar radiation forecasting. *Theoretical and Applied Climatology*, *137*(1-2), 31-43. https://doi.org/10.1007/s00704-018-2576-4.

Cao, Y., Liu, G., Luo, D., Bavirisetti, D. P., & Xiao, G. (2023). Multi-timescale photovoltaic power forecasting using an improved Stacking ensemble algorithm based LSTM-Informer model. *Energy*, *283*. https://doi.org/10.1016/j.energy.2023.128669.

Cryer, J. D., & Chan, K.-S. (s.d.). *Springer Texts in Statistics Time Series Analysis With Applications in R Second Edition*.

Dairi, A., Harrou, F., Sun, Y., & Khadraoui, S. (2020). Short-term forecasting of photovoltaic solar power production using variational auto-encoder driven deep learning approach. *Applied Sciences (Switzerland)*, *10*(23), 1-20. https://doi.org/10.3390/app10238400.

Dhaked, D. K., Dadhich, S., & Birla, D. (2023). Power output forecasting of solar photovoltaic plant using LSTM. *Green Energy and Intelligent Transportation*, *2*(5). https://doi.org/10.1016/j.geits.2023.100113.

El Robrini, F., & Amrouche, B. (2023). Support Vector Regression for Predicting Intra-day Photovoltaic Generation in Algeria. In *International Conference on Electronics, Energy, and Measurement*. Medea. https://doi.org/10.1109/IC2EM59347.2023.10419659.

El Robrini, F., Bukhari, S. M. S., Zafar, M. H., Al-Tawalbeh, N., Akhtar, N., & Sanfilippo, F. (2024). Federated learning and non-federated learning based power forecasting of photovoltaic/wind power energy systems: A systematic review. *Energy and AI*, *18*, 100438. https://doi.org/10.1016/j.egyai.2024.100438.

Feroz Mirza, A., Mansoor, M., Usman, M., & Ling, Q. (2023). Hybrid Inception-embedded deep neural network ResNet for short and medium-term PV-Wind forecasting. *Energy Conversion and Management*, *294*. https://doi.org/10.1016/j.enconman.2023.117574.

Gandhi, O., Kumar, D. S., Rodríguez-Gallegos, C. D., & Srinivasan, D. (2020a). Review of power system impacts at high PV penetration Part I: Factors limiting PV penetration. *Solar Energy*, *210*, 181-201. https://doi.org/10.1016/j.solener.2020.06.097.

Gandhi, O., Kumar, D. S., Rodríguez-Gallegos, C. D., & Srinivasan, D. (2020b). Review of power system impacts at high PV penetration Part I: Factors limiting PV penetration. *Solar Energy*, *210*, 181-201. https://doi.org/10.1016/j.solener.2020.06.097.

Geng, D., Wang, B., & Gao, Q. (2023). A hybrid photovoltaic/wind power prediction model based on Time2Vec, WDCNN and BiLSTM. *Energy Conversion and Management*, *291*. https://doi.org/10.1016/j.enconman.2023.117342.

Guermoui, M., Bouchouicha, K., Bailek, N., & Boland, J. W. (2021a). Forecasting intra-hour variance of photovoltaic power using a new integrated model. *Energy Conversion and Management*, *245*. https://doi.org/10.1016/j.enconman.2021.114569.

Guermoui, M., Gairaa, K., Boland, J., & Arrif, T. (2021b). A Novel Hybrid Model for Solar Radiation Forecasting Using Support Vector Machine and Bee Colony Optimization Algorithm: Review and Case Study. *Journal of Solar Energy Engineering, Transactions of the ASME*, *143*(2). https://doi.org/10.1115/1.4047852.

Hamza Zafar, M., Mujeeb Khan, N., Mansoor, M., Feroz Mirza, A., Kumayl Raza Moosavi, S., & Sanfilippo, F. (2022). Adaptive ML-based technique for renewable energy system power forecasting in hybrid PV-Wind farms power conversion systems. *Energy Conversion and Management*, *258*. https://doi.org/10.1016/j.enconman.2022.115564.

Harrou, F., Kadri, F., & Sun, Y. (2020). Forecasting of Photovoltaic Solar Power Production Using LSTM Approach. Dans F. Harrou (Éd.), *Advanced Statistical Modeling, Forecasting, and Fault Detection in Renewable Energy Systems*. (S.l.) : IntechOpen. https://doi.org/10.5772/intechopen.91248.

Hassan, M. A., Bailek, N., Bouchouicha, K., & Nwokolo, S. C. (2021). Ultra-short-term exogenous forecasting of photovoltaic power production using genetically optimized non-linear auto-regressive recurrent neural networks. *Renewable Energy*, *171*, 191-209. https://doi.org/10.1016/j.renene.2021.02.103.

Hosseini Dolatabadi, S. H., Soleimani, A., Maghanaki, M., & Ilinca, A. (2024). Enhancing Photovoltaic Farm Capacity Estimation: A Comprehensive Analysis with a Novel Approach. *Energy Technology*, *12*(4). https://doi.org/10.1002/ente.202301294.

Huang, J., Korolkiewicz, M., Agrawal, M., & Boland, J. (2013). Forecasting solar radiation on an hourly time scale using a Coupled AutoRegressive and Dynamical System (CARDS) model. *Solar Energy*, *87*(1), 136-149. https://doi.org/10.1016/j.solener.2012.10.012.

Keddouda, A., Ihaddadene, R., Boukhari, A., Atia, A., Arıcı, M., Lebbihiat, N., & Ihaddadene, N. (2023). Solar photovoltaic power prediction using artificial neural network and multiple regression considering ambient and operating conditions. *Energy Conversion and Management*, *288*. https://doi.org/10.1016/j.enconman.2023.117186.

Khelifi, R., Guermoui, M., Rabehi, A., & Lalmi, D. (2020). Multi-step-ahead forecasting of daily solar radiation components in the Saharan climate. *International Journal of Ambient Energy*, *41*(6), 707-715. https://doi.org/10.1080/01430750.2018.1490349.

Khelifi, R., Guermoui, M., Rabehi, A., Taallah, A., Zoukel, A., Ghoneim, S. S. M., … Zaitsev, I. (2023). Short-Term PV Power Forecasting Using a Hybrid TVF-EMD-ELM Strategy. *International Transactions on Electrical Energy Systems*, *2023*. https://doi.org/10.1155/2023/6413716.

Kuppusamy, M., & Balaraman, S. (2024). Long Short Term Memory Tracker-Based Modified DC-DC Converter for Power Quality Improvement in Grid-PV Systems under Uniform and Partial Shading Environments. *Energy Technology*, *12*(3). https://doi.org/10.1002/ente.202300648.

Kushwaha, V., & Pindoriya, N. M. (2019). A SARIMA-RVFL hybrid model assisted by wavelet decomposition for very short-term solar PV power generation forecast. *Renewable Energy*, *140*, 124-139. https://doi.org/10.1016/j.renene.2019.03.020.

Liu, Q., Darteh, O. F., Bilal, M., Huang, X., Attique, M., Liu, X., & Acakpovi, A. (2023). A cloud-based Bi-directional LSTM approach to grid-connected solar PV energy forecasting for multi-energy systems. *Sustainable Computing: Informatics and Systems*, *40*. https://doi.org/10.1016/j.suscom.2023.100892.

Mamdouh, M., Ezzat, M., & Hefny, H. (2024). Improving flight delays prediction by developing attention-based bidirectional LSTM network. *Expert Systems with Applications*, *238*. https://doi.org/10.1016/j.eswa.2023.121747.

Mansoor, M., Feroz Mirza, A., Usman, M., & Ling, Q. (2023). Hybrid forecasting models for wind-PV systems in diverse geographical locations: Performance and power potential analysis. *Energy Conversion and Management*, *287*. https://doi.org/10.1016/j.enconman.2023.117080.

Rabehi, A., Guermoui, M., & Lalmi, D. (2020). Hybrid models for global solar radiation prediction: a case study. *International Journal of Ambient Energy*, *41*(1), 31-40. https://doi.org/10.1080/01430750.2018.1443498.

Raza, M. Q., Nadarajah, M., & Ekanayake, C. (2016, 15 octobre). On recent advances in PV output power forecast. *Solar Energy*. Elsevier Ltd. https://doi.org/10.1016/j.solener.2016.06.073.

Sadeghi, D., Golshanfard, A., Eslami, S., Rahbar, K., & Kari, R. (2023). Improving PV power plant forecast accuracy: A hybrid deep learning approach compared across short, medium, and long-term horizons. *Renewable Energy Focus*, *45*, 242-258. https://doi.org/10.1016/j.ref.2023.04.010.

Sahin, G., Isik, G., & van Sark, W. G. J. H. M. (2023). Predictive modeling of PV solar power plant efficiency considering weather conditions: A comparative analysis of artificial neural networks and multiple linear regression. *Energy Reports*, *10*, 2837-2849. https://doi.org/10.1016/j.egyr.2023.09.097.

Sampath Kumar, D., Gandhi, O., Rodríguez-Gallegos, C. D., & Srinivasan, D. (2020). Review of power system impacts at high PV penetration Part II: Potential solutions and the way forward. *Solar Energy*, *210*, 202-221. https://doi.org/10.1016/j.solener.2020.08.047.

Shab, G. (2022). *Prévision multi-horizon de l'éclairement global horizontal pour la gestion intelligente du réseau électrique de distribution en région Occitanie*. Université de Perpignan.

Ssekulima, E. B., Anwar, M. B., Al Hinai, A., & El Moursi, M. S. (2016, 1 juillet). Wind speed and solar irradiance forecasting techniques for enhanced renewable energy integration with the grid: A review. *IET Renewable Power Generation*. Institution of Engineering and Technology. https://doi.org/10.1049/iet-rpg.2015.0477.

Thaker, J., & Höller, R. (2024). Hybrid model for intra-day probabilistic PV power forecast. *Renewable Energy*, *232*, 121057. https://doi.org/10.1016/j.renene.2024.121057.

Wang, F., Xuan, Z., Zhen, Z., Li, K., Wang, T., & Shi, M. (2020). A day-ahead PV power forecasting method based on LSTM-RNN model and time correlation modification under partial daily pattern prediction framework. *Energy Conversion and Management*, *212*. https://doi.org/10.1016/j.enconman.2020.112766.

Wu, F., Wang, S., Liu, D., Cao, W., Fernandez, C., & Huang, Q. (2024). An improved convolutional neural network-bidirectional gated recurrent unit algorithm for robust state of charge and state of energy estimation of new energy vehicles of lithium-ion batteries. *Journal of Energy Storage*, *82*. https://doi.org/10.1016/j.est.2024.110574.

Yang, D. (2019). Making reference solar forecasts with climatology, persistence, and their optimal convex combination. *Solar Energy*, *193*, 981-985. https://doi.org/10.1016/j.solener.2019.10.006.

Ziane, A., Necaibia, A., Sahouane, N., Dabou, R., Mostefaoui, M., Bouraiou, A., … Blal, M. (2021). Photovoltaic output power performance assessment and forecasting: Impact of meteorological variables. *Solar Energy*, *220*, 745-757. https://doi.org/10.1016/j.solener.2021.04.004.

Web sites :

Bilan des Capacités d'Energies Renouvelables Installées en Algérie à Fin 2023. (2024). Algeria. https://www.cerefe.gov.dz/wp-content/uploads/2024/09/Bilan-des-secteurs-jusqua-fin-2023_.pdf.

Commissariat aux Energies Renouvelables et à l'Efficacité Energétique. (2020). Transition Energétique en Algérie. www.cerefe.gov.dz.

Ministère de la Transition Energétique et des Energies Renouvelables. (2021, 26 novembre). AVIS D'APPEL D'OFFRES A INVESTISSEURS N°01/MTEER/2021.

SONELGAZ-EnR. (2023, 27 février). NATIONAL AND INTERNATIONAL OPEN TO TENDER N°01:CEEG/2023. *BAOSEM EDITION & PUBLICITE*. https://moit.gov.vn/upload/2005517/fck/files/Thong_tin_moi_thau_xay_dung_15_nha_may_dien_mat_troi_2226c.pdf.